This article has been accepted for publication in a future issue of this journal, but has not been fully edited. Content may change prior to final publication. Citation information: DOI 10.1109/JSAC.2021.3064640, IEEE Journal on Selected Areas in Communications

Analogue Coherent-Optical Mobile Fronthaul with Integrated Photonic Beamforming

Dinka Milovančev, *Member, IEEE,* Nemanja Vokić, *Member, IEEE,* David Löschenbrand, *Student Member, IEEE,* Thomas Zemen, *Senior Member, IEEE,* and Bernhard Schrenk, *Member, IEEE*

***Abstract*— We present a mobile fronthaul methodology for the analogue optical transmission of native radio signals with integrated photonic true-time delay for the beam steering of phased-array antennas. Laser-based coherent homodyne detectors and the delay dissemination through ultra-dense wavelength division multiplexing ensure a low complexity at the optical layer. We experimentally demonstrate beamsteering for a linear phased-array antenna with a 1×3 configuration at 3.5 GHz carrier frequency and prove native radio signal transmission over the 14.3-km reach coherent optical fronthaul at a low end-to-end error vector magnitude of 3.3%. Experimental results are found to stand in good agreement with theoretical predictions.**

***Index Terms*—Optical communication terminals, 5G, Optical signal detection, Mobile fronthaul, RF Beamforming, Microwave photonics**

I. Introduction

OPTICAL front- and backhaul networks have been adopted in modern 5G communication networks [1]. These optical links enable cloud-based radio access network (RAN) architectures where signal processing functions are efficiently pooled at a dedicated processing warehouse or mobile edge computing cloudlets [2]. This way of laying out the RAN ensures cost- and energy-efficient handling of radio signals, while it also allows for interference mitigation. At the same time, this RAN architecture overlaps with the consolidation efforts of optical wireline access. Under the umbrella of wireline-wireless convergence [3], the same fiber infrastructure may serve both aspects of fixed and mobile data transmission over fiber (or hybrid fiber-copper) and air, respectively.

The optical relaying of wireless signals over the fronthaul of the RAN has to preserve the signal integrity of the radio signals. Since opto-electronic signal conversion is prone to signal degradation due to non-linearity and noise, the optical radio signal transmission is often performed in the digital domain [4,5] and may even involve front-end digital signal processing (DSP) functions at the antenna site. This means that the radio signal has to be digitized before optical transmission, incurring oversampling and a high resolution to avoid error floors due to analogue-to-digital and digital-to-analogue (ADC/DAC) conversion functions. As such, the digital fronthaul effectively spoils the idea of centralizing digital functions: ADC/DAC (and optional DSP) functions must be again distributed at the antenna sites in the field, thus offsetting the cost- and energy-efficiency inherent to the cloud-RAN concept.

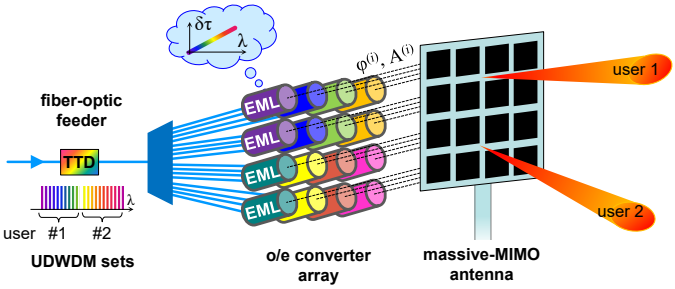

Fig. 1. Optical fronthaul architecture with delay dissemination implemented in the UDWDM dimension, and coherent EML receivers performing delay selection for each of the independently steered antenna elements.

In an attempt to find a trade-off for this implementation problem, various split options have been defined [1]. These options move more and more functions of the radio stack towards the cloud hostel, to eventually arrive at an analogue optical fronthaul that does not involve any ADC/DAC or DSP functions at the antenna site. Therefore, the complexity of field- and mass-deployed remote radio heads (RRH) remains relatively low. Analogue radio-over-fiber schemes [6] are now being intensively researched [7, 8] for this reason and have proven to be practically feasible.

Besides antenna remoting and centralized baseband processing, antenna schemes building on multiple inputs and multiple outputs (MIMO) and the support for higher carrier frequencies are considered a key enabler for a migration from cell-centric to beam-centric radio access [9]. The formation of radio beams in mm-wave massive MIMO configurations is achieved through shifting the phase of the radio carrier frequency, preferably through a programmable true-time delay associated to each antenna element. Radio frequency (RF) based beamforming networks can easily become complex, are typically laid out for a specific carrier frequency and very

Manuscript received July 1, 2020. This work was supported in part by the European Research Council (ERC) under the European Union's Horizon 2020 research and innovation programme (grant agreement No 804769) and by the Austrian Research Promotion Agency FFG through the TRITON project (grant agreement No 858697).

D. Milovancev, N. Vokic, D. Löschenbrand, T. Zemen and B. Schrenk are with the AIT Austrian Institute of Technology, Center for Digital Safety&Security, Giefinggasse 4, 1210 Vienna, Austria (phone: +43 50550-4131; fax: -4150; e-mail: bernhard.schrenk@ait.ac.at).

limited signal bandwidth and their inclusion at the antenna site further complicates the centralized RF management. For these reasons, transparent photonic RF beamforming methods compatible with high signal bandwidths and fast tuning response are of high interest.

The scientific contribution of this work is the advancement of a conceptually simple analogue radio-over-fiber transmission scheme, introduced earlier [10], towards analogue coherent optical RF beamforming. We accomplish this task without altering the optical distribution network and without dedicated beamformer circuitry at the antenna site. Instead, we employ an electro-absorption modulated laser (EML) as coherent receiver, which enables us to introduce ultra-dense wavelength division multiplexing (UDWDM) as an optical dimension for signal aggregation. We extend our previous findings by exploiting the UDWDM concept with a low-complexity coherent receiver for the purpose of true-time delay dissemination to eventually integrate photonics-enabled RF beamsteering with the mobile optical fronthaul.

The paper is organized as follows. Section II discusses the state-of-the-art in photonic-assisted RF beamforming methods and relates the current work to it. Section III introduces the beamforming concept that is integrated with the analogue mobile fronthaul. Section IV elaborates on the experimental arrangement, while Section V provides the results obtained for RF beamsteering. Section VI investigates the transmission performance for analogue radio-over-fiber transmission over the proposed beamforming architecture. Finally, Section VII concludes the work.

II. State-of-the-Art in True-Time Delays and Photonic-Assisted RF Beamformers

A variety of analogue solutions for optical phase shifting and, more importantly, true-time delays (TTD) has been investigated in the past years [11-45], with the aim to leverage wide and flat bandwidths that are known for microwave photonics. Besides offering a large operating bandwidth, these microwave and mm-wave functions shall ideally be continuously tunable over a large delay range with a fast settling time between different operational set points, and shall be as transparent as possible, both in terms of optical loss, wavelength range and radio signal waveform.

There are many principles that can be exploited for realizing a TTD in the optical domain. Differential delays can be introduced through spatial switching or tuning of the propagation path [11-20] or transmission over a dispersive medium for which its wavelength-dependent dispersion slope suffices the required amount of phase delay [21-30]. Switched binary delays realized through fiber-optic [12, 14, 19, 20, 23] or waveguide-based delay lines [31, 32] lead to a discretization of the obtained delay, which is an undesired characteristic for 5G beamforming. Contrarily, wavelength-tuned transmission over media featuring chromatic dispersion, such as single-mode fiber [21, 25, 28] or linearly chirped Bragg gratings [22, 24, 27, 30], provides a continuous delay setting, yet it requires a precise and stable optical source. Given the typically high bandwidth that is supported by opto-electronics, low RF carrier frequencies become more challenging since rather long delay lines or highly dispersive media are required. Continuous delay settings can also be obtained using bulk optical assemblies that build on a tunable path delay through internal reflection mechanisms [11, 17] or spatial light modulators that enable arbitrary phase shifts [16]. Alternatively, highly compact elements that offer a tunable group delay at resonance, such as micro resonators [31-37] or waveguide gratings [38-40] can be directly implemented in InP, SiN or silicon-on-insulator based integrated circuits. A combination of switched binary delays and a smaller continuous delay element enables larger delays of up to 1.8 ns [32]. Tuning is obtained through a slower thermo-optic with 7 µs response time [34], wavelength tuning using a fast tunable laser [13], or an inherently fast electro-optic effect with a settling time in the nanosecond range [12, 41]. Table I summarizes a wider range of demonstrations, which are not exclusively built on the aforementioned methods.

The availability of TTD elements allows to shape beamforming networks, which, as introductorily stated, are recognized as key building blocks in emerging radio access networks. Nonetheless, a rather small number of RF beamforming networks has been experimentally demonstrated. While early practical implementations have relied on fiber- [19, 21, 26-29] or bulk optics [16] for this purpose, the emergence and maturity of photonic integration platforms have allowed to drastically improve the compactness and scalability of TTD functions [14, 31, 33-40, 45] and beamforming networks [12, 20, 41]. The fractional signal bandwidth can greatly determine the complexity of a scaled up beamformer, since phase shifters become compatible constituent elements for narrow signal bandwidths and can be generally realized with lower complexity than advanced TTD functions. System-level performance with large bandwidth of more than 40 GHz [12, 17, 18, 24, 33, 41, 43] or support for high RF carrier frequencies of 93 GHz [20] has been eventually demonstrated, proving also compatibility with rapid beamsteering at switching times of 1 ns [27, 41] and small footprint for the beamforming network.

All of the previous works rely on simple and proven PIN photoreceivers to convert the optically transmitted radio signal back to the electrical domain. We instead propose to use coherent rather than direct detection. Coherent detection typically leads to a radio frequency shift since the local optical oscillator (LO) and the optical source at the transmitter are free-running and thus in general not synchronized. Despite this implementation challenge, we will extend our preliminary investigation on an UDWDM-based antenna feed [46] and will experimentally demonstrate that RF beamforming can be achieved without requiring DSP, which would actually contradict the efforts of providing an analogue beamforming solution. The adoption of low-complexity coherent detection offers numerous benefits. Unlike in the RF domain, optical spectrum is abundant and can be used in broadcast-and-select architectures that build on an ultra-dense WDM methodology. We will exploit such an architecture in combination with the chromatic dispersion of the fronthaul for the purpose of delay dissemination, which together with comb transmission and coherent reception obviates the need for precise tunable lasers and tunable filters. Moreover, coherent detection can compensate for the optical losses in virtue of its sensitivity

TABLE I
EXPERIMENTAL TRUE-TIME DELAY, PHASE-SHIFTER AND BEAMFORMING DEMONSTRATIONS

Ref.	Year	Principle for TTD / phase shifter	Scan type	Beam-forming exp/(sim)	Compactness	Optical loss	Bandwidth (signal width)	Delay range (step size)	Steering angle	Tuning speed
[11]	2002	internal path reflection	discr.	-	bulk optical path reflector, 4.6 mm high	N/A	18 - 26.5 GHz (2.5 Gb/s)	443 ps	±36°	1μs
[12]	2006	switched delay	discr.	1×4	InP PIC (8 × 10 mm^2)	27-21 dB	42.7 GHz (155Mb/s QAM)	15.7 (2.2) ps	-47.7°	5 ns
[21]	2005	PCF	cont.	1×4	Fiber-optics (PCF)	3.4 dB	X band	±31 ps	23°	-
[13]	2008	fiber mirror array	discr.	(1×32)	Fiber-optics (fiber mirror, WDM demux)	5-7 dB	>12 GHz BW (1 GHz FM)	300 ns	±61°	<1 μs (laser)
[22]	2008	chirped FBG	cont.	-	fiber-optics (FBG)	7.4 dB	1 to 18 GHz	1 ns	±60°	-
[23]	2009	switched FBG	discr.	-	fiber-optics (optical switches, FBG)	N/A	1 GHz	409 ps	-	-
[33]	2010	cascade of coupled MRRs	cont.	-	SOI PIC, 3.35 mm long (235 MRRs)	17 dB off-chip	380 GHz	0.73 ps per MRR	-	-
[14]	2010	switched delay	discr.	-	SOI PIC (3.5 × 1.5 cm^2)	< 6dB	X band	2.5 ns	-	<1 μs
[42]	2010	Brillouin scattering	cont.	(32×32)	fiber-optics (DSF)	N/A	0.1 GHz at 6 GHz	10 ns	±45°	-
[43]	2010	PMF-based DI	cont.	(1×5)	Fiber-optics (PMF, PBS)	N/A	60 GHz	33.3 ps	90°	-
[24]	2011	chirped FBG	cont.	-	fiber-optics (FBG)	N/A	56 GHz	200 ps	-	-
[15]	2011	MEMS mirrors	discr.	-	16 × 5 × 4 $inch^3$ benchtop	10.22 dB	20 GHz	25 (0.3) ns	-	<100 μs
[16]	2011	liquid crystal on silicon	cont.	1×4	Bulk optics (LCoS, diffraction grating)	N/A	10 GHz BW	0 to 2π	±40° (18 GHz)	-
[34]	2012	MRR array	cont.	-	SOI PIC, 0.9 mm long (20 MRRs)	~24dB	30 - 40 GHz (10.5 GHz pulse)	345 ps	-	7.2 μs (thermal)
[17]	2013	internal path reflection	cont.	-	optical path reflector. 64 lines: 12 × 17 × 8.4 cm^3	<1 dB	40 GHz	30 ns	-	500 μs
[25]	2014	SMF / reconfigurable filter	discr.	-	Fiber-optics (SMF) + programmable filter	N/A	12 GHz	1.4 (0.07) ns	-	filter tuning
[35]	2014	MRR	cont.	-	SiN PIC	1.2 dB (on-chip)	3–7 GHz	0.3 ns	-	thermal
[38]	2014	reflective waveguide grating	cont.	-	SOI PIC (130 μm long)	23 dB (off-chip)	10 GHz	19.4 ps	160° (22-29 GHz)	-
[26]	2015	DCF	cont.	1×2	Fiber-optics (DCF)	N/A	0.3 GHz at 5.9, 12.7, 17 GHz	±200 ps	-22 to 29°	laser tuning
[18]	2015	heterogeneous MCF	discr.	-	fiber-optics (7-core MCF)	N/A	100 GHz	100 ps (typ.)	-	-
[44]	2015	DI with phase shifter	cont.	-	Fiber-optics (PMF, phase modulator)	N/A	10 GHz	31.9 ps	-	33 μs
[27]	2016	chirped FBG in recirculating loop	cont.	1×4	Fiber-optics (FBG)	active loop	11.2 GHz	2.5 ns/trip	±60°	<1 ns
[36]	2016	MRR	cont.	-	SOI PIC (167 × 230 μm^2)	13 dB	30.5 GHz	72 ps	-	pn junction
[39]	2016	waveguide grating array	discr.	-	SOI PIC (8 × 0.5 mm^2)	~11 dB off-chip	20 GHz (10 GHz pulse)	30 (10) ps	-	-
[41]	2016	plasmonic phase modulator	cont.	1×4	Si plasmonic PIC (800 × 550 μm^2)	~18.5 dB	narrow (1 Gbaud QPSK at 60 GHz)	-	30°	1 ns
[45]	2017	Brillouin scattering	cont.	-	chalcogenide PIC (2.4 × 0.930 μm^2)	4.8 dB	0.1 GHz	4 ns	-	-
[28]	2017	DCF array	cont.	1×8	fiber-optics (DCF array)	N/A	9.5 to 10.5 GHz	-	43°	12.5 ns
[31]	2017	switched delay + MRR	cont.	-	SOI PIC (5.4 × 5.3 mm^2)	12.4 dB on-chip	60 GHz (30 Gb/s OOK)	1.28 ns	-	19 μs
[37]	2017	MRR	cont.	-	SiN PIC (8 × 32 mm^2)	10 dB (off-chip)	8.7 GHz (3 Gb/s OOK at 41 GHz)	172.4 ps	49°	-
[29]	2018	chirped FBG cascade	cont.	1×4	Fiber-optics (FBG)	N/A	2 - 10 GHz	104 ps	±17.8°	-
[19]	2018	variable ODL + MCF feed	cont.	1×8	Fiber-optics (ODL, MCF)	N/A	V band (14 Gb/s bonded QAM)	±16.6 ps	30°	-
[40]	2018	waveguide grating	cont.	-	SOI PIC (0.18 mm^2)	N/A	X-band	300 ps	±67.84°	72.3°/μs
[20]	2019	Switched delay	discr.	1×4	SiN PIC (8 × 32 mm^2)	N/A	W band (93 GHz)	steps 1.5 ps	-51 to 31°	thermal
[32]	2019	switched delay / MRR array	discr. / cont.	-	SiN PIC (~1 × 2.4 cm^2)	2.5 dB (on-chip)	17.6 to 21.2 GHz	1.8 ns	-	-
[30]	2020	chirped FBG array	cont.	1×4	Fiber-optics (FBG)	N/A	X + Ku bands	±250 ps	±36.8°	-

Abbreviations used in this table: DCF dispersion compensating fiber, DI delay interferometer, FBG fiber Bragg grating, InP Indium-Phosphide, LCoS liquid crystal on silicon, MCF multi-core fiber, MRR micro-ring resonator, ODL optical delay line, PCF photonic crystal fiber, PBS polarization beam splitter, SiN silicon nitride, SMF single-mode fiber, SOI silicon on insulator

This article has been accepted for publication in a future issue of this journal, but has not been fully edited. Content may change prior to final publication. Citation information: DOI 10.1109/JSAC.2021.3064640, IEEE Journal on Selected Areas in Communications

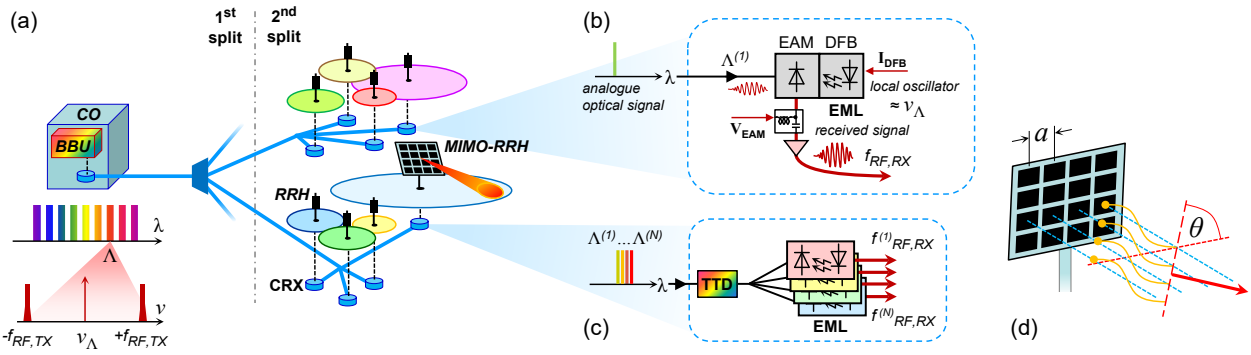

Fig. 2. (a) Optical fronthaul architecture with delay dissemination implemented in the UDWDM dimension, exploiting coherent homodyne receivers for (b) single-element RRHs and (c) arrayed RRH configuration with preceding TTD implemented optically. (d) Beamsteering with phased array antenna.

gain. With these, beamforming functionality can be conveniently integrated with the analogue radio-over-fiber transmission at the mobile fronthaul.

Cost-wise, extra components that are required for the integration of RF beamforming and that exceed what is fundamentally required for the optical fronthaul, such as optical transmitters, receivers, the transmission fiber and passive splitting functions as required to operate a multi-element RRH over a single, cost-shared feeder lane, will raise the cost inefficiency of a solution. According to this basic and widely agreed principle of minimizing capital expenditures, earlier work that employs specialized fibers, dispersion-tailored components or other fiber-optic bulk components [13, 21-24, 43] will likely be associated to higher cost when compared with concepts that leverage photonic integrated circuit (PIC) technology that augments the opto-electronic RRH transceiver front-end with optically-enabled RF beamforming functions [12, 14, 33-41]. Towards this second direction, the largest cost contribution of PIC-based solutions derives from assembly and packaging [47]. It is therefore essential to reduce the number of fiber ports and electrical pins. The concept proposed in this work fits squarely, as it requires a minimum number of optical or electrical connections by virtue of its low-complexity coherent receiver with single fiber port and its realization of the RF beamforming function through the transmission medium in combination with coherent detection.

III. Fronthaul with Integrated RF Beamforming

The proposed coherent mobile fronthaul with integrated RF beamforming relies on three key ingredients, which are introduced in this Section and highlighted in Fig. 1: *(i)* delay dissemination through UDWDM in combination with *(ii)* the TTD contributed by the dispersive fronthaul feeder, and *(iii)* low-complexity coherent detection for filterless delay selection.

A. UDWDM Fronthaul with Wavelength-Set Partitioning

Figure 2(a) presents the optical fronthaul architecture on which the proposed concept builds. Radio signals are passed between the baseband units (BBU) hosted at the central office (CO) and the RRHs at the antenna sites. Analogue radio-over-fiber transmission is the option of choice, since the entire RF management can be centralized. Paramount to such an approach are analogue opto-electronic transmitters and receivers [48], which stand in contradiction to the traditional use of digital optical transmission systems that deal with low-complexity modulation formats such as on-off keying.

The optical distribution network between the CO and the RRHs serves as point-to-multipoint fronthaul. A high number of RRHs is linked to the CO by means of UDWDM. An antenna site may either host a small number of RRHs or, in case of a site with beamforming capability, a larger number of RRHs. Such a beamforming-assisted site that is entirely controlled in its amplitude A and phase φ by the CO does greatly benefit from analogue transmission of the native radio waveform, as shall be evidenced from a comparison with digitized radio signal relay: Assuming a bandwidth of up to 1 GHz for carrier-aggregated radio, a resolution of 12 bits and a 2-fold oversampling for the ADC/DAC, and N antenna elements, the CPRI-equivalent data rate of the directly digitized radio signal at its carrier frequency amounts to $N \times$ 24 Gb/s per sector prior to channel coding and can easily reach into the Tb/s regime [49].

Passive branching devices at the optical fronthaul network distribute the feeder signal of the CO towards the RRHs and combine the RRH signals vice versa. Two splitting stages are foreseen for this purpose: The first splitter distributes optical spectrum among different antenna sites. This can be facilitated in a colorless manner through a passive power split or, considering a relaxation for the link loss budget, by means of dense WDM. In either case a portion of spectrum with multiple tightly-spaced UDWDM channels can be allocated to each antenna site. In this way a virtual point-to-point link is established for each RRH element rather than macro-cell site. This densification in connectivity is accomplished through occupation of abundant optical spectrum. This available spectrum results from the optical whitespace between the dense WDM overlay as specified for 5G fronthauling [50]. The second splitter at the antenna site is employed to feed the associated coherent receivers (CRX) that are linked to the RRHs in a broadcast-and-select and therefore colorless and filterless fashion.

Such an UDWDM methodology is known from wired optical access and has been identified as feasible [51], provided that the tail-end transceiver sub-systems at the

This article has been accepted for publication in a future issue of this journal, but has not been fully edited. Content may change prior to final publication. Citation information: DOI 10.1109/JSAC.2021.3064640, IEEE Journal on Selected Areas in Communications

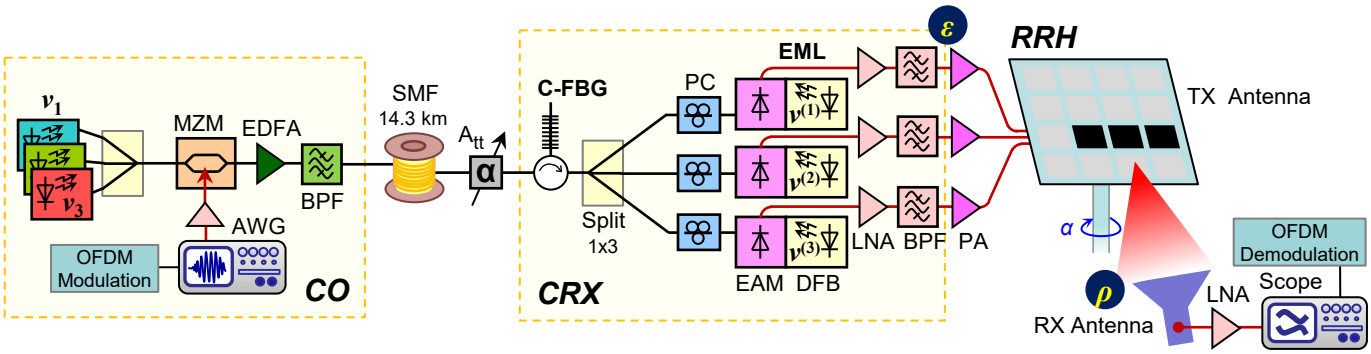

Fig. 3. Experimental setup of the optical fronthaul with integrated photonic beamsteering.

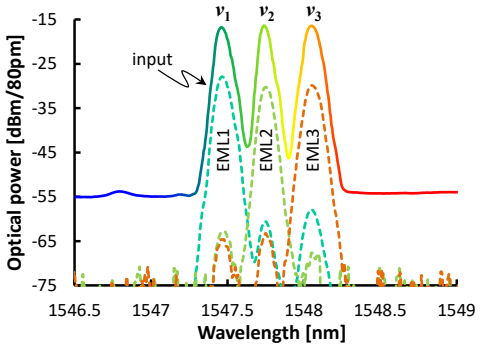

Fig. 4. Optical spectra showing the transmitted UDWDM channels and the tapped EML outputs when the LOs are locked on all three channels.

RRHs, where no cost-sharing applies, can be realized with a reasonable complexity. This aspect will be addressed in Section III.B. Each of the optical UDWDM slices, as sketched in Fig. 2(a) for the case of wavelength Λ and the corresponding optical emission frequency ν_Λ, is modulated with a radio signal at its RF carrier frequency $f_{RF,TX}$. Coherent detection not only replaces the optical filters otherwise needed for channel selection, but also compensates the colorless power-splitting loss through its sensitivity gain.

The transceivers employed at CO and RRH are laid out for analogue radio-over-fiber transmission. A transparent translation of the radio signals from the electrical to the optical domain, and vice versa, is endeavored in terms of low signal degradation due to noise or non-linearity, but also in terms of frequency preservation. The latter is of special interest when employing coherent detection, as endeavored in this work, since a free-running LO is to be incorporated as an optical synthesizer with unstable frequency and phase.

B. Coherent Homodyne Detection with Laser Receiver

Coherent detection is considered the enabler of an UDWDM architecture, which is associated to spectral efficiency and high optical budgets in virtue of the selectivity and sensitivity obtained through coherent reception. Yet, the practical implementation of coherent optical receivers is a complex exercise. The poor quality of optical sources in terms of frequency and phase stability, together with the uncontrolled polarization along a fiber-based lightpath, typically requires DSP functions to mitigate these optical layer impairments [52]. However, this renders the radio-over-fiber system one more time as a digital implementation.

Figure 2(b) presents the alternative analogue coherent reception engine that is employed as the downlink receiver at the RRH. It essentially consists of an EML as a very compact single-polarization coherent receiver [53]. The incoming radio signal at wavelength $\Lambda^{(1)}$ is detected by the electro-absorption modulator (EAM), which serves as photodiode when biased at absorption. The distributed feedback laser (DFB) of the same EML is also absorbed by the EAM and hence, it beats with the radio signal. For this purpose, the emission frequency of the DFB is tuned to ν_Λ. Since the emission frequencies of the downlink transmitter at the CO and the EML at the RRH will generally differ, coherent intradyne detection applies. With this the received radio signal will appear at an RF carrier frequency $f_{RF,RX} \approx f_{RF,TX}$. This means that the radio carrier frequency is changed and that optical double-sideband modulation leads to signal fading unless DSP is employed.

In order to mitigate this shortcoming, the DFB laser is injection locked by the optical carrier of the received optical radio signal [54]. To do so, the DFB laser emission is tuned through temperature or current control over a range of ~3 nm, with the aim of locating it within the locking range of the incident radio signal. This frequency difference, in which locking occurs, is typically 200 MHz at -30 dBm [53]. Once the DFB is locked, the wavelength of the received signal and the LO match precisely, leading to $f_{RF,RX} = f_{RF,TX}$. This case of coherent homodyne detection leads to translation of the radio signal from the optical to the electrical domain while ensuring high signal integrity. In addition to our previous works, we further prove the compatibility with simpler double-sideband modulation at the optical downlink.

It shall be stressed that a tandem-EML is required for polarization-independent operation [55]. Due to the scarcity of available EML devices for a multi-element antenna feed, the experiment has been conducted using manual polarization control in combination with a single-polarization EML.

C. Delay Dissemination for True-Time Delay Selection

The implementation of a multi-channel true-time delay by means of photonics and, in particular, integrated with the optical fronthaul, is considered an important aspect for further simplification of the RRH equipment. In this work, we exploit the already present optical transmission fiber as dispersive

This article has been accepted for publication in a future issue of this journal, but has not been fully edited. Content may change prior to final publication. Citation information: DOI 10.1109/JSAC.2021.3064640, IEEE Journal on Selected Areas in Communications

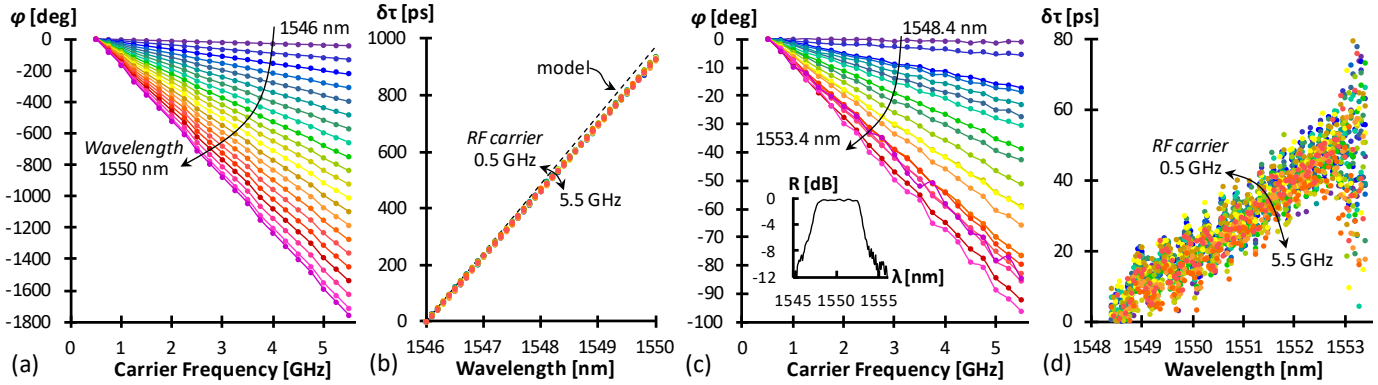

Fig. 5. Introduced (a) RF phase shift and (b) delay for the SMF fronthaul feeder. (c) RF Phase shift for the C-FBG and corresponding delay (d).

element for this purpose, similar as in [25], and therefore as a shared TTD element. In this way, a wavelength-dependent delay is obtained and the relative phase shift in the RF domain is controlled through choice of the emission frequency of the optical carrier. However, in case that multiple antenna elements are to be fed, the respective signals need to be demultiplexed, a process that can face scalability issues as the number of radio-over-fiber sub-channels increases.

UDWDM fits squarely to such a TTD scheme as it enables us to feed multiple antenna elements and allows for a fine granularity in terms of delay setting. Compared to [25], no complex filters are required, which eases the scalability towards a higher number of sub-channels.

In the proposed concept for delay dissemination, the selected channel of the UDWDM broadcast can be associated to a certain delay δτ (Fig. 1). This delay is chosen by locking the LO $\nu_{(i)}$ of the receiver independently on the respective UDWDM channel $\Lambda^{(i)}$. In case of a beamforming RRH array with linear antenna configuration, for which the CRX is presented in Fig. 2(c), the optical LO frequencies $\nu_{(1)}\ldots\nu_{(N)}$ are determining the phase shift at the antenna element. This relative phase among the particular RF signals that feed the elements of the phased array antenna will lead to a beam steering angle according to the well-known relation

$$\theta = \arcsin\left(\frac{c\,\delta\tau}{a}\right) \tag{1}$$

where c is the speed of light and a is the distance between two antenna elements, as sketched in Fig. 2(d). With $\lambda_{(i)}$ being the corresponding optical wavelength associated to the optical frequency $\nu_{(i)}$ of the LO, D the dispersion coefficient of the fronthaul feeder, L its length and λ_L the lower cut-off wavelength for the DFB tuning range, the homodyne reception through the EML yields

$$\theta = \arcsin\left(\frac{cDL}{a}\left(\lambda_{(i)} - \lambda_L\right)\right) \tag{2}$$

For a linear antenna with N elements, the LO wavelengths will be accordingly chosen with $\lambda_{(i)} = i \cdot \Delta\lambda + \lambda_L$, in order to realize the respective phase shift φ between the RF carriers at consecutive antenna elements. The spacing $\Delta\lambda$ can be constant, according to a UDWDM broadcast with fixed wavelength grid, but can also be flexible, as it would be the case in a grid-less UDWDM scheme.

The injection locking methodology introduced in Section III.B, together with a multi-line transmission of radio-over-fiber signals, can alleviate the beamforming network from precise tunable lasers, which are considered a complex element. By choosing a fixed spacing between comb lines, small enough to obtain a quasi-continuous delay tuning, the complexity for the optical power supply reduces to a single laser without precise wavelength alignment. This is because the relative difference between delay set-points is now determined by a stable RF tone used to generate the optical frequency comb, while the locking range of the EML receivers is large enough to obtain stable locking [54]. However, as Section V.C will discuss, a grid-based UDWDM scheme will impose a discretization that, in case of a large number of antenna elements, leads to a step size in beam steering that exceeds the beam width. In such a case, a grid-less UWDM scheme can offer a continuous delay tuning, at the expense of a more complicated wavelength control at the CO.

UDWDM in combination with coherent reception with a simple and compact detector for every antenna element does also offer a high degree of flexibility. For example, the same UDWDM channel can be used by multiple receivers due to the filterless split architecture, which can raise the optical spectral efficiency in case of 1-dimensional beamforming. More importantly, multiple beams can be realized at a single RRH array by dedicating multiple, adjacent UDWDM wavelength sets to the same antenna site (Fig. 1). In such a case UDWDM sets do not necessarily relay the same radio signal over the fronthaul but are instead associated to different data streams.

It shall also be stressed that it is possible to control not only the RF phase but also the RF amplitude of the radio signal. This possibility of setting the delivered power to the antenna element through the EAM bias of the coherent EML receiver [54] is seen as an important aspect towards sidelobe level control and therefore interference mitigation in mm-wave massive-MIMO systems [56].

This article has been accepted for publication in a future issue of this journal, but has not been fully edited. Content may change prior to final publication. Citation information: DOI 10.1109/JSAC.2021.3064640, IEEE Journal on Selected Areas in Communications

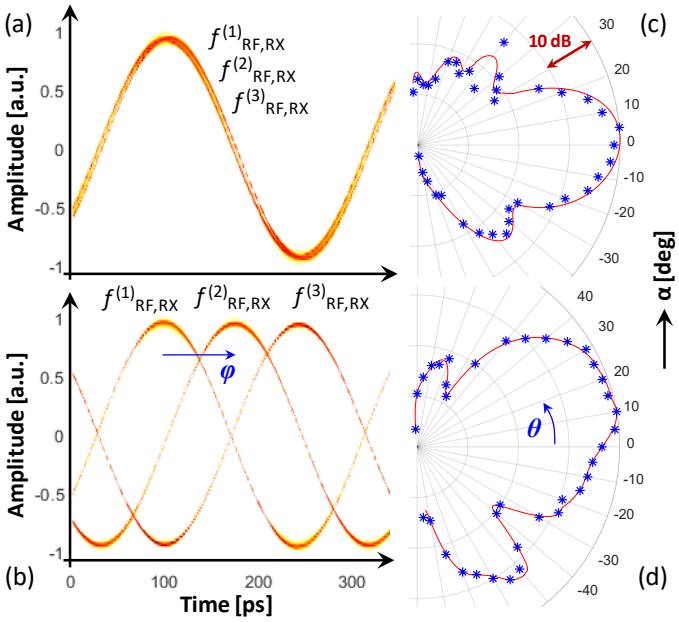

Fig. 6. Fronthauling of three identical RF carriers at 3.5 GHz with EML-based coherent homodyne detectors in case of reception at (a) the same and (b) different UDWDM channels. The respective impact of the introduced phase shift φ on the beam pattern emitted by the phased-array transmit antenna is shown in (c) an (d).

IV. Experimental Setup

The experimental setup to prove the downlink transmission for the proposed coherent analogue fronthaul with integrated photonic beamsteering for a 1×3 antenna configuration is shown in Fig. 3. At the CO a 125-MHz orthogonally frequency division multiplexed (OFDM) radio signal at a carrier f_{RF} = 3.5 GHz with 128 sub-carriers is modulated as double-sideband signal on three closely spaced optical carriers $v_1 \ldots v_3$ in the vicinity of 1548 nm (Fig. 4). The UDWDM wavelength set is boosted, launched with 3 dBm/λ at an OSNR of 37.2 dB/0.1nm, and fed to the antenna site through a 14.3 km single-mode fiber (SMF) span, which complies with the latency requirements of cloud-RAN architectures. At the CRX for the multi-element antenna, each of the elements is dedicated to an EML-based coherent detector. Transistor-outline EMLs for 1548.51 nm were employed for this purpose and a 50Ω low-noise amplifier has been used as RF front-end. Although this is sub-optimal in terms of reception performance, it is unavoidable as a transimpedance amplifier cannot be co-integrated with the EML detector due to the transistor-outline package. The DFBs of the EMLs, which represent the LOs, are independently locked on the three UDWDM channels. In a different setting, they will be locked on the same channel. The time delay between the UDWDM channels is determined by the SMF and is further tailored by a dedicated linearly chirped fiber Bragg grating (C-FBG), which is introduced at the CRX. This grating had a center wavelength of 1550.1 nm, a bandwidth of 5.7 nm, a reflectivity of 99.2% and a length of ~20 nm. Manual polarization controllers have been inserted before the single-polarization EMLs, as discussed earlier. The input power to the EMLs was -18.7 dBm/λ. The output of the EMLs are amplified, filtered by a bandpass at 3.59 GHz with a bandwidth of 2.2 GHz, and boosted to the 1×3 arrangement of a multi-element phased-array antenna that was designed for a carrier frequency of 3.5 GHz. Its beam is analyzed through a high-directivity receive antenna, which has an antenna gain of 23 dB and is placed 1.5 m apart from the transmit antenna. In this way multi-path interference effects are suppressed, while the beam steering capability of the RF transmitter can be analyzed through rotating the transmit antenna by an azimuth α.

V. Photonic RF Beamsteering

A. Fronthaul-integrated TTD

The delay obtained through photonic RF signal transmission has been analyzed by means of end-to-end fronthaul link characterization using a vector network analyzer after opto-electronic conversion with a PIN receiver. Figure 5(a) shows the RF phase shift for exclusive transmission over the SMF feeder for various wavelengths in the range of 1546 to 1550 nm. Clearly, the phase shift is high enough to allow for wide angle tuning, as it is also evident from the delay of up to 930 ns is obtained over the tuning range, as presented in Fig. 5(b). More importantly, the accomplished delay, which is a linear function of the wavelength, is independent of the RF carrier frequency. This renders the SMF as a TTD that can be used as a shared element to construct an RF beamformer, as introduced in Fig. 1. Since the main lobe of a so-formed antenna beam will orientate into the same direction for different RF frequencies, squint-free operation is obtained. The delay also agrees well with the model $\delta\tau = DL(\lambda - \lambda_L)$, with λ_L = 1546 nm, for which a dispersion coefficient of 17 ps/(nm km) was assumed for the SMF.

In the case that antenna sites are very closely located to the CO, the feeder length might be too short to introduce the required amount of delay. In this case, a C-FBG can be a compact alternative. Figure 5(c) reports the introduced RF phase shift for various wavelengths within the C-FBG reflection window, which is shown as inset. Although the shift shows a ripple and its extent is clearly less than for the 14.3 km SMF, a delay of up to 50 ps can be supported at the end of the C-FBG reflection window (Fig. 5(d)). This delay would correspond to a ±4.9° steering angle at a RF carrier frequency of 5.9 GHz and a 4-element antenna, which is too narrow to cover an entire 120° sector. However, beamsteering can be supported in case of elevated RF carrier frequencies such as they are used in the mm-wave bands.

It shall be stressed that dynamic delay tuning is to be supported in order to track moving objects or to swiftly switch between different end-users. Injection locking can be in principle supported for a delay- and thus wavelength-swept input data signal, as it has been experimentally validated for the proposed EML-based coherent receiver for a small wavelength detuning [57].

B. RF Beamsteering

The PIN receiver has then been substituted by the EML

This article has been accepted for publication in a future issue of this journal, but has not been fully edited. Content may change prior to final publication. Citation information: DOI 10.1109/JSAC.2021.3064640, IEEE Journal on Selected Areas in Communications

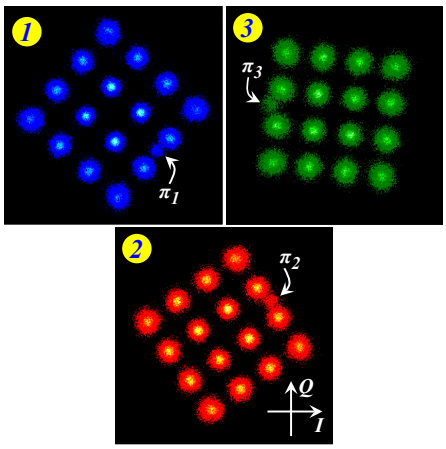

Fig. 7. OFDM constellations received at the three EMLs feeding three antenna elements.

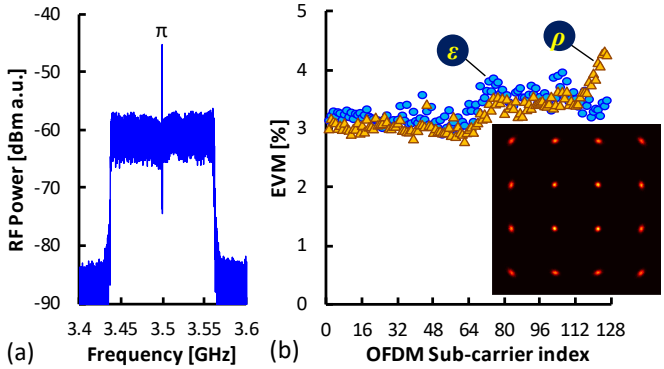

Fig. 8. (a) Received OFDM signal after coherent homodyne detection with an EML, and (b) EVM performance at EML output after optical fronthaul transmission (ε) and additional RF propagation (ρ). The constellation is shown at the EML receiver output as aggregated QAM over all sub-carriers.

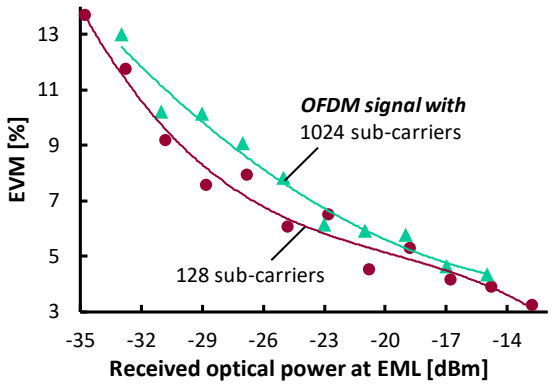

Fig. 9. Error vector magnitude for 16-QAM OFDM transmission for a 128 and 1024 sub-carrier loaded radio signal.

receivers and all three optical carriers ν_i have been modulated by the same 3.5-GHz RF carrier. Figure 6 shows the received RF carriers $f^{(i)}_{RF,RX}$ at the EML outputs (point ε in Fig. 3). In the first case, presented in Fig. 6(a), all three EMLs lock on the central carrier ν_2. This is possible since the 1×3 splitter at the CRX enables a filterless broadcast-and-select scheme. There is no phase difference between the RF carriers since there is no wavelength detuning, meaning that the RF beam will be emitted without steering. In the second case, presented in Fig. 6(b), the EMLs are individually locked on the three different optical carriers, which follow the UDWDM spacing of $\Delta\lambda$ = 0.29 nm, as indicated in the inset of Fig. 4. The detuning leads to an experimentally confirmed relative phase shift of φ = 73° between the RF carriers, which is clearly visible in Fig. 6(b) and which agrees well with the expected value of 74.7° for the actual UDWDM channel spacing. For the given antenna, $a = 0.6\,\xi$, with ξ being the wavelength associated to the RF carrier frequency of 3.5 GHz. With a relative delay of 73° between two RF carriers, we expect a steering by $\theta^* = 19.8°$.

Figure 6 further reports the beam pattern as emitted by the phased-array transmit antenna. In order to obtain this characteristic, the transmit antenna has been rotated by an angle α while the high-directivity receive antenna has been kept fixed. For the equiphase feed with φ = 0 between the antenna elements, which is presented in Fig. 6(c) and corresponds to Fig. 6(a), the beam delivers its highest power at α = 0. When the relative phase shift φ of Fig. 6(b) is applied, the beam steers by $\theta \approx 20°$, as it is reported in Fig. 6(d). This agrees well with the expected angle θ^*.

C. Continuity in Beamsteering

A delay dissemination scheme that builds on a comb with fixed UDWDM spacing will introduce a lower limit for the beam steering continuity. If we assume simple double-sideband optical modulation, a RF carrier frequency of 3.5 GHz and the obtained delay over SMF-based fronthaul, Eq. (2) yields a step size of 4° for the beam steering angle. This step size is smaller than the typical beamwidth [58] expected for corresponding 8×8 element antenna configurations. In case of spectrally efficient single-sideband UDWDM analogue radio-over-fiber transmission, the step size falls below the beamwidth of 16×16 antennas. If a truly continuous steering is required, a more elaborated spectral management that alleviates the UDWDM setup from a fixed, equidistant channel spacing needs to be implemented. In such an approach, the delay is no longer disseminated in a broadcast-and-select methodology, but selectively transmitted.

VI. Analogue Radio Transmission Performance

The transmission performance has been evaluated for a 16-ary quadrature amplitude modulated (QAM) OFDM radio signal transmission in order to reliably retrieve larger error vector magnitude (EVM) values at high RF path loss resulting from off-centric beam measurements. The received OFDM signal spectrum after reception by an EML receiver (ε) is shown in Fig. 8(a). Coherent homodyne optical detection ensures that the RF carrier frequency is preserved, which is evidenced by the sharp pilot tone π at 3.5 GHz and the clear boundaries of the OFDM spectrum. The radio signal has been acquired by a real-time oscilloscope and has been offline demodulated. No further DSP functions have been applied besides bandpass filtering.

Phase discrimination of the OFDM pilot π with a local RF reference can serve the auxiliary monitoring of the RF phase

This article has been accepted for publication in a future issue of this journal, but has not been fully edited. Content may change prior to final publication. Citation information: DOI 10.1109/JSAC.2021.3064640, IEEE Journal on Selected Areas in Communications

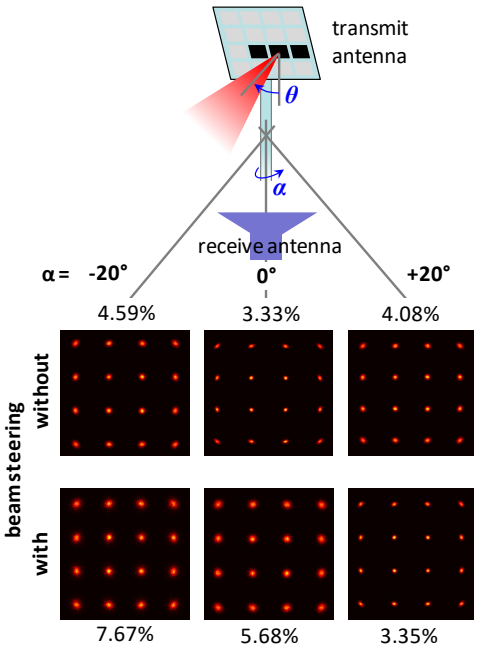

Fig. 10. Received constellations and averaged EVM over all sub-carriers after optical fronthauling and RF propagation as function of the rotation angle α of the transmit antenna, in absence and presence of beamsteering.

shift and wavelength-control of the optical receiver. Figure 7 demonstrates an example for three OFDM constellations after opto-electronic conversion for the EML locked at $\nu_{(1)}\ldots\nu_{(3)}$. Phases of -39.5°, 35°, and 170.3° are measured for the pilots $\pi_1 ... \pi_3$. These values indicate proper alignment for channels 1 and 2 for the aforementioned case, while channel 3 is still misaligned.

In order to evaluate the transparency of the optical fronthaul with integrated RF beamforming to the radio signal, the EVM performance for the OFDM sub-carriers is presented in Fig. 8(b). A low average EVM of 3.37% (●) far below the EVM antenna limit is obtained. The received constellation of the radio signal proves this point. This confirms that the coherent optical fronthaul with low-complexity opto-electronics is able to preserve the signal integrity, and does therefore not limit the reception performance of the native radio signal.

Figure 9 shows the EVM of the 16-QAM OFDM signal as function of the received optical power at an EML receiver at the RRH. The EVM over all 128 sub-carriers reaches an average value that corresponds to the antenna limit of 12.5% for at a received power of -33.8 dBm (●). Comparison is also made with an OFDM signal that is composed of 1024 sub-carriers (▲), which shows a penalty of 0.8 dB at the antenna limit that is attributed to the increased peak-to-average power ratio. The obtained sensitivities lead to a compatible loss budget of 35.6 dB. Taking into account end-of-life fiber transmission loss at the feeder, a large power margin of 31.6 dB remains to be eroded by the loss of the optical splitter placed at the RRH to distribute the UDWDM signal to the coherent receivers feeding the antenna elements.

Finally, EVM measurements have been conducted by manually altering the angle α of the transmit antenna in absence and presence of a relative phase φ between the

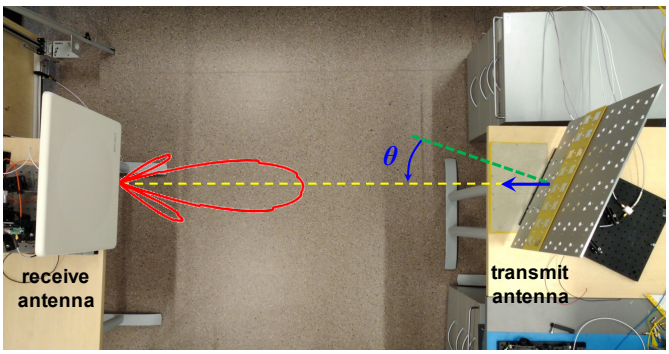

Fig. 11. Transmit antenna setup for optimal radio signal transmission under 20° beamsteering.

elements of its phased-array configuration. Figure 10 presents the obtained EVM and constellations as function of α after RF propagation (point ρ in Fig. 3). Without beam steering, meaning that all EMLs lock on the same UDWDM channel ν_2, a minimum average EVM of 3.33% is obtained at $\alpha = 0$, since $\theta = 0$. The respective EVM performance is included in Fig. 8(b,▲). When the transmit antenna is rotated by $\alpha = -20°$, the EVM worsens up to 4.6%. With present beamsteering due to EML locking to different UDWDM channels $\nu_1 \ldots \nu_3$, the minimum EVM is now obtained when the transmit antenna is rotated by 20° and is found with 3.35%. Figure 11 shows a top-view of the antenna constellations for this case. At the original face-to-face alignment of transmit and receive antenna ($\alpha = 0$), the EVM increases to 5.68% and worsens rapidly for negative α. These results resemble the photonically set deflection angle θ.

VII. Conclusion

We exploited the tunability of EMLs as analogue coherent optical homodyne detectors to support true-time delay functionality integrated with an analogue optical fronthaul. Wavelength partitioning in a broadcast-and-select UDWDM in combination with dispersive media allowed to set a shift in the RF carrier phase, which was eventually applied in a phased-array antenna configuration to steer the beam for radio signal transmission. Experimental beamsteering by 20° has been shown for a 14.3-km fronthaul link in good agreement to the theoretical model, with negligible EVM penalty for 16-QAM OFDM reception at 3.5 GHz carrier frequency.

Migration towards mm-wave frequencies in combination with a broadband EML receiver is left for future work. Moreover, the ability of a single EML to serve as bidirectional transceiver, as demonstrated in recent proof-of-concept demonstrations, may prove beneficial with respect to the presented RF beamforming architecture.

References

[1] I.A. Alimi, A.L. Teixeira, and P.P. Monteiro, "Toward an Efficient C-RAN Optical Fronthaul for the Future Networks: A Tutorial on Technologies, Requirements, Challenges, and Solutions," *IEEE Comm. Surveys & Tutorials*, vol. 20, no. 1, pp. 708-769, 2018.

[2] C. Pan, M. Elkashlan, J. Wang, J. Yuan, and L. Hanzo, "User-Centric C-RAN Architecture for Ultra-Dense 5G Networks: Challenges and Methodologies," *IEEE Comm. Mag.*, vol. 56, no. 6, pp. 14-20, 2017.

[3] J.I. Kani, J. Terada, K.I. Suzuki, and A. Otaka, "Solutions for Future Mobile Fronthaul and Access-Network Convergence," *IEEE/OSA J. Lightwave Technol.*, vol. 35, no. 3, pp. 527-534, Feb. 2017.

[4] X. Liu, H. Zeng, N. Chand, and F. Effenberger, "Efficient Mobile Fronthaul via DSP-based Channel Aggregation," *IEEE/OSA J. Lightwave Technol.*, vol. 34, no. 6, pp. 1556-1564, Mar. 2016.

[5] T. Pfeiffer, "Next Generation Mobile Fronthaul and Midhaul Architectures," *IEEE/OSA J. Opt. Comm. Netw.*, vol. 7, no. 11, pp. B38-B45, 2015.

[6] J. Beas, G. Castanon, I. Aldaya, A. Aragon-Zavala, and G. Campuzano, "Millimeter-Wave Frequency Radio over Fiber Systems: A Survey," *IEEE Comm. Surveys & Tutorials*, vol. 15, no. 4, pp. 1593-1619, 2013.

[7] H.N. Parajuli *et al.*, "Experimental demonstration of multi-Gbps multi sub-bands FBMC transmission in mm-wave radio over a fiber system," *OSA Opt. Expr.*, vol. 26, no. 6, pp. 7306-7312, 2018.

[8] N. Argyris *et al.*, "A 5G mmWave Fiber-Wireless IFoF Analog Mobile Fronthaul Link With up to 24-Gb/s Multiband Wireless Capacity," *IEEE/OSA J. Lightwave Technol.*, vol. 37, no. 12, pp. 2883-2891, Feb. 2020.

[9] S.A. Busari, K.M.S. Huq, S. Mumtaz, L. Dai, and J. Rodriguez, "Millimeter-Wave Massive MIMO Communication for Future Wireless Systems: A Survey," *IEEE Comm. Surveys & Tutorials*, vol. 20, no. 2, pp. 836-869, 2018.

[10] B. Schrenk, "The EML as Analogue Radio-over-Fiber Transceiver – a Coherent Homodyne Approach," *IEEE/OSA J. Lightwave Technol.*, vol. 37, no. 12, pp. 2866-2872, Jun. 2019.

[11] C. Yihong, and R.T. Chen, "A fully packaged true time delay module for a K-band phased array antenna system demonstration," *IEEE Phot. Technol. Lett.*, vol. 14, no. 8, pp. 1175-1177, Aug. 2002.

[12] M.A. Piqueras *et al.*, "Optically beamformed beamswitched adaptive antennas for fixed and mobile broadband wireless access networks," *IEEE Trans. Microwave Theory and Tech.*, vol. 54, no. 2, pp. 887-898, Feb. 2006.

[13] O. Raz, S. Barzilay, R. Rotman, and M. Tur, "Submicrosecond Scan-Angle Switching Photonic Beamformer With Flat RF response in the C and X Bands," *IEEE/OSA J. Lightwave Technol.*, vol. 26, no. 15, pp. 2774-2781, Aug. 2008.

[14] S. Fathpour, and N.A. Riza, "Silicon-photonics-based wideband radar beamforming: Basic design", *Optical Engineering*, vol. 49, no. 1, p. 018201, Jan. 2010.

[15] B.L. Anderson *et al.*, "Hardware demonstration of extremely compact optical true time delay device for wideband electronically steered antennas," *IEEE/OSA J. Lightwave Technol.*, vol. 29, no. 9, pp. 1343–1353, May 2011.

[16] X. Yi, T.X.H. Huang, and R.A. Minasian, "Photonic Beamforming Based on Programmable Phase Shifters With Amplitude and Phase Control," *IEEE Photon. Technol. Lett.*, vol. 23, no. 18, pp. 1286-1288, Sep. 2011

[17] S.R. Davis, S.T. Johnson, S.D. Rommel, and M.H. Anderson, "Next Generation Photonic True Time Delay Devices as Enabled by a New Electro-Optic Architecture," *Proc. of SPIE, Sensors and Systems for Space Applications VI*, vol. 8739, 2013.

[18] S. Garcia, and I. Gasulla, "Design of heterogeneous multicore fibers as sampled true-time delay lines," *OSA Opt. Lett.*, vol. 40, no. 4, pp. 621-624, Feb. 2015.

[19] T. Nagayama, S. Akiba, T. Tomura, and J. Hirokawa, "Photonics-Based Millimeter-Wave Band Remote Beamforming of Array-Antenna Integrated With Photodiode Using Variable Optical Delay Line and Attenuator," *IEEE/OSA J. Lightwave Technol.*, vol. 36, no. 19, pp. 4416-4422, Oct. 2018.

[20] Y. Liu, B. Isaac, J. Kalkavage, E. Adles, T. Clark, and J. Klamkin, "93-GHz Signal Beam Steering with True Time Delayed Integrated Optical Beamforming Network," in Proc. *Opt. Fib. Comm. Conf.*, San Diego, United States, Mar. 2019, Th1C.5.

[21] Y. Jiang *et al.*, "Dispersion-enhanced photonic crystal fiber array for a true time-delay structured X-band phased array antenna," *IEEE Phot. Technol. Lett.*, vol. 17, no. 1, pp. 187-189, Jan. 2005.

[22] B. Zhou, X. Zheng, X. Yu, H. Zhang, Y. Guo, and B. Zhou, "Optical Beamforming Networks Based on Broadband Optical Source and Chirped Fiber Grating," *IEEE Photon. Technol. Lett.*, vol. 20, no. 9, pp. 733-735, May 2008.

[23] B.M. Jung, and J. Yao, "A two-dimensional optical true time-delay Beamformer consisting of a fiber Bragg grating prism and switch-based fiber-optic delay lines," *IEEE Phot. Technol. Lett.*, vol. 21, no. 10, pp. 627-629, May 2009.

[24] H. Shahoei, M. Li, and J.P. Yao, "Continuously tunable time delay using an optically pumped linearly chirped fiber Bragg grating," *IEEE/OSA J. Lightwave Technol.*, vol. 29, no. 10, pp. 1465-1472, May 2011.

[25] X. Ye, F. Zhang, and S. Pan, "An Optical True-Time-Delay Unit for Multi-Beamforming," *OSA Opt. Expr.*, vol. 23, no. 8, pp. 10002-10008, Apr. 2015.

[26] D.H. Yang, and W.P. Lin, "Phased-array beam steering using optical true time delay technique," *Optics Communication*, vol. 350, pp. 90-96, Mar. 2015.

[27] J. Zhang, and J. Yao, "Photonic true-time delay Beamforming using a switch-controlled wavelength-dependent recirculating loop," *IEEE/OSA J. Lightwave Technol.*, vol. 34, no. 16, pp. 3923-3929, Aug. 2016.

[28] L. Zhang *et al.*, "Photonic true time delay beamforming technique with ultra-fast beam scanning," *OSA Opt. Expr.*, vol. 25, no. 13, pp. 14524-14532, Jun. 2017.

[29] J. Zhao, Z. Ding, F. Yang, and H. Cai, "Configurable Photonic True-Time Delay Line Based On Cascaded Linearly Chirped Fiber Bragg Grating," in *Proc. Int. Topical Meeting on Microwave Phot.*, Toulouse, France, Oct. 2018, pp. 1-4.

[30] N.K. Srivastava, R. Parihar, and S. K. Raghuwanshi, "Efficient Photonic Beamforming System Incorporating a Unique Featured Tunable Chirped Fiber Bragg Grating for Application Extended to the Ku-Band," *IEEE Trans. Microwave Theory and Tech.*, vol. 68, no. 5, pp. 1851-1857, Feb. 2020.

[31] X. Wang, L. Zhou, R. Li, J. Xie, L. Lu, K. Wu, and J. Chen, "Continuously tunable ultra-thin silicon waveguide optical delay line," *OSA Optica*, vol. 4, no. 5, pp. 507-515, May 2017.

[32] I. Visscher *et al.*, "Broadband True Time Delay Microwave Photonic Beamformer for Phased Array Antennas," in Proc. Europ. Conf. Antennas and Propagation, Krakow, Poland, Mar. 2019, pp. 1-5.

[33] M.L. Cooper *et al.*, "Statistics of light transport in 235-ring silicon coupled-resonator optical waveguides," *OSA Opt. Expr.*, vol. 18, no. 25, pp. 26505-26516, Dec. 2010.

[34] P.A. Morton, J. Cardenas, J.B. Khurgin, and M. Lipson, "Fast thermal switching of wideband optical delay line with no long-term transient," *IEEE Photon. Technol. Lett.*, vol. 24, no. 6, pp. 512-514, Mar. 2012.

[35] L. Zhuang *et al.*, "On-chip microwave photonic beamformer circuits operating with phase modulation and direct detection," *OSA Opt. Expr.*, vol. 22, no. 14, pp. 17079-17091, Jul. 2014.

[36] W. Zhang, and J. Yao, "Electrically tunable silicon-based on-chip microdisk resonator for integrated microwave photonic applications," *APL Photonics*, vol. 1, p. 080801, 2016.

[37] Y. Liu *et al.*, "Ultra-Low-Loss Silicon Nitride Optical Beamforming Network for Wideband Wireless Applications," *IEEE/OSA J. Lightwave Technol.*, vol. 24, no. 4, p. 8300410, Jul. 2018.

[38] M. Burla, L.R. Cortes, M. Li, X. Wang, L. Chrostowski, and J. Azana, "On-chip programmable ultra-wideband microwave photonic phase shifter and true time delay unit," *OSA Opt. Lett.*, vol. 39, no. 21, pp. 6181-6184, Nov. 2014.

[39] J. Wang *et al.*, "Subwavelength grating enabled on-chip ultra-compact optical true time delay line," *Sci. Rep.*, vol. 6, p. 30235, 2016.

[40] G. Wang *et al.*, "Continuously tunable true-time delay lines based on a one-dimensional grating waveguide for beam steering in phased array antennas," *Appl. Opt.*, vol. 57, no. 18, pp. 4998-5003, Jun. 2018.

[41] R. Bonjour *et al.*, "Plasmonic phased array feeder enabling ultrafast beam steering at millimeter waves," *OSA Opt. Expr.*, vol. 24, no. 22, pp. 25608-25618, Oct. 2016.

[42] S. Chin *et al.*, "Broadband true time delay for microwave signal processing, using slow light based on stimulated Brillouin scattering in optical fibers," *OSA Opt. Expr.*, vol. 18, no. 21, pp. 22599-22613, Oct. 2010.

[43] M.V. Drummond, P.P. Monteiro, and R.N. Nogueira, "Photonic True-Time Delay Beamforming Based on Polarization-Domain Interferometers," *IEEE/OSA J. Lightwave Technol.*, vol. 28, no. 17, pp. 2492-2498, Sep. 2010.

[44] R. Bonjour, S.A. Gebrewold, D. Hillerkuss, C. Hafner, and J. Leuthold, "Continuously tunable true-time delays with ultra-low settling time", *OSA Opt. Expr.*, vol. 23, no. 5, pp. 6952-6964, Mar. 2015.

[45] I. Aryanfar *et al.*, "Chip-based Brillouin radio frequency photonic phase shifter and wideband time delay," *OSA Opt. Lett.*, vol. 42, no. 7, pp. 1313-1316, Apr. 2017.

[46] D. Milovancev, N. Vokic, D. Löschenbrand, T. Zemen, and B. Schrenk, "Analogue Radio-Over-Fiber Fronthaul with UDWDM-based Delay Dissemination for Photonic-Assisted RF Beam Steering," in *Proc. Europ. Conf. Opt. Comm.*, Brussels, Belgium, Dec. 2020, Th.2G.7.

[47] T. Barwidz *et al.*, "Automated, high-throughput photonic packaging," *Opt. Fib. Technol.*, vol. 44, pp. 24-35, 2018.

[48] K. Xu *et al.*, "Microwave photonics: radio-over-fiber links, systems, and applications," *Photon. Res.*, vol. 2, pp. B54-B63, 2014.

[49] N. Suzuki, H. Miura, K. Matsuda, R. Matsumoto, and K. Motoshima, "100 Gb/s to 1 Tb/s Based Coherent Passive Optical Network Technology," *IEEE/OSA J. Lightwave Technol.*, vol. 36, no. 8, pp. 1485-1491, Apr. 2018.

[50] *"40-Gigabit-capable passive optical networks 2 (NG-PON2): Physical media dependent (PMD) layer specification,"* ITU-T Recommendation G.989.2, Dec. 2014.

[51] H. Rohde *et al.*, "Trials of a Coherent UDWDM PON Over Field-Deployed Fiber: Real-Time LTE Backhauling, Legacy and 100G Coexistence," *IEEE/OSA J. Lightwave Technol.*, vol. 33, no. 8, pp. 1644-1649, Apr. 2015.

[52] S.J. Savory, "Digital Coherent Optical Receivers: Algorithms and Subsystems," *IEEE J. Sel. Topics in Quantum Electron.*, vol. 16, no. 5, pp. 1164-1179, Sep. 2010.

[53] B. Schrenk, and F. Karinou, "A Coherent Homodyne TO-Can Transceiver as Simple as an EML," *IEEE/OSA J. Lightwave Technol.*, vol. 37, no. 2, pp. 555-561, Jan. 2019.

[54] B. Schrenk, "Injection-Locked Coherent Reception Through Externally Modulated Laser," *IEEE J. Sel. Topics in Quantum Electron.*, vol. 24, no. 2, p. 3900207, Mar. 2018.

[55] B. Schrenk, and F. Karinou, "Simple Laser Transmitter Pair as Polarization-Independent Coherent Homodyne Detector," *OSA Opt. Expr.*, vol. 27, no. 10, pp. 13942-13950, May 2019.

[56] T.L. Marzetta, "Noncooperative Cellular Wireless with Unlimited Numbers of Base Station Antennas," *IEEE Trans. Wireless Comm.*, vol. 9, no. 11, pp. 3590-3600, Nov. 2010.

[57] B. Schrenk, "Synchronized Wavelength-Swept Signal Transmission and its Ability to Evade Optical Reflection Crosstalk", *OSA Opt. Lett.*, vol. 44, no. 11, pp. 2771-2774, Jun. 2019.

[58] M. Plotkin, "Beamwidth of Phased Arrays," *IEEE Trans. Ant. and Prop.*, vol. 21, no. 5, pp. 695-697, Sep. 1973.

Dinka Milovančev (M'19) was born in Serbia in 1990. She finished her M.Sc. studies in 2014 in Microelectronics from the University of Novi Sad, Serbia. She obtained her Ph.D. degree at Vienna University of Technology in Austria at the Institute of Electrodynamics, Microwave and Circuit Engineering in 2019. Her Ph.D. research was focused on circuit design of integrated avalanche photodiode receivers and their applications for optical wireless and fiber communication. Since 2019 she is employed at AIT Austrian Institute of technology, Vienna, where she works in the field of coherent optical fiber communication in classical as well as quantum optical domain.

Nemanja Vokić (M'19) was born in Serbia in 1990. He received the M.Sc. degree in electrical and computer engineering from the University of Novi Sad, Serbia in 2014. He obtained his Ph.D. degree from Vienna University of Technology in 2018. For his Ph.D. work, he designed full-custom electronic integrated circuits for transmitters and receivers used for optical communications. He was then a post-doc at Vienna University of Technology, designing mm-wave ASICs for 5G remote radio heads. In 2019, he joined AIT Austrian Institute of Technology, Vienna. His research interests include design of analog and RF integrated circuits, opto-electronic circuit integration, coherent optical communication for telecom, datacom and quantum communications.

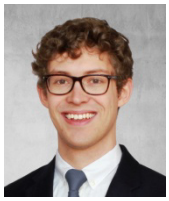

David Löschenbrand (S'19) received the Dipl.-Ing. degree (with distinction) in Telecommunications in 2016 from Vienna University of Technology. From 2012 to 2015, he worked for the Institute of Telecommunications, implementing software for antenna characterization purposes. Since 2016, he is a Ph.D. candidate with the Austrian Institute of Technology in the group of Thomas Zemen. His research interests focus on massive MIMO in time-varying propagation channels, channel aging, antenna design, reliable low-latency wireless communications for highly autonomous vehicles, vehicular channel measurements and channel modelling. He successfully implemented a software defined radio based massive MIMO testbed for highspeed measurements and signal processing experimentation, which provides crucial insights for several ongoing research projects.

Thomas Zemen (S'03-M'05-SM'10) received the Dipl.-Ing. degree (with distinction) in electrical engineering in 1998, the doctoral degree (with distinction) in 2004 and the Venia Docendi (Habilitation) for "Mobile Communications" in 2013, all from Vienna University of Technology.
Dr. Zemen is Principal Scientist at AIT Austrian Institute of Technology, Vienna, Austria, leading the reliable wireless communications group. He joined AIT in 2014 and took on the role of thematic coordinator for physical layer security in 2017. From 2003 to 2014 he was with FTW Forschungszentrum Telekommunikation Wien heading the "Signal and Information Processing" department since 2008. From 1998 to 2003 Thomas Zemen worked as hardware engineer and project manager for the radio communication devices department, Siemens Austria. He has authored four books chapters, 37 journal papers, more than 112 conference communications and two patents. His research interest focuses on the interplay of the physical wireless radio communication channel with other parts of a communication system in time-critical applications.
Dr. Zemen is an External Lecturer with the Vienna University of Technology and served as Editor for the IEEE Transactions on Wireless Communications from 2011 – 2017.

Bernhard Schrenk (S'10-M'11) was born 1982 in Austria and received the M.Sc. ('07) degree in microelectronics from the Technical University of Vienna. He was at the Institute of Experimental Physics of Prof. A. Zeilinger, where he was involved in the realization of a first commercial prototype for a quantum cryptography system, within the European SECOQC project. From 2007 to early 2011 he obtained his Ph.D degree at UPC BarcelonaTech, Spain. His Ph.D thesis on multi-functional optical network units for next-generation Fiber-to-the-Home access networks was carried out within the FP7 SARDANA and EURO-FOS projects. In 2011 he joined the Photonic Communications Research Laboratory at NTUA, Athens, as post-doctoral researcher and established his research activities on coherent FTTH under the umbrella of the FP7 GALACTICO project. In 2013 he established his own research force on photonic communications at AIT Austrian Institute of Technology, Vienna, where he is working towards next-generation metro-access-5G networks, photonics integration technologies and quantum optics.
Dr. Schrenk has authored and co-authored ~180 publications in top-of-the-line (IEEE, OSA) journals and presentations in the most prestigious and highly competitive optical fiber technology conferences. He was further awarded with the Photonics21 Student Innovation Award and the Euro-Fos Student Research Award for his PhD thesis, honoring not only his R&D work but also its relevance for the photonics industry. He was elected as Board-of-Stakeholder member of the Photonics21 European Technology Platform in 2017. During his extensive research activities he was and is still engaged in several European projects such as SARDANA, BONE, BOOM, APACHE, GALACTICO, EURO-FOS and the Quantum Flagship project UNIQORN. In 2013 he received the European Marie-Curie Integration Grant WARP-5. In 2018 he was awarded by the European Research Council with the ERC Starting Grant COYOTE, which envisions coherent optics everywhere.